Weierstraß-Institut
für Angewandte Analysis und Stochastik
Leibniz-Institut im Forschungsverbund Berlin e. V.

Preprint ISSN 0946 – 8633

A tangential regularization method for backflow stabilization in hemodynamics

Cristóbal Bertoglio[1], Alfonso Caiazzo[2]

submitted: June 18, 2013

[1] Institute for Computational Mechanics
Technische Universität München
85747 Garching b. München
Germany
E-Mail: bertoglio@lnm.mw.tum.de

[2] Weierstrass Institute
Mohrenstr. 39
10117 Berlin
Germany
E-Mail: Alfonso.Caiazzo@wias-berlin.de

No. 1800
Berlin 2013

2010 *Mathematics Subject Classification.* 62P10, 76D05, 76M10, 76Z05.

2010 *Physics and Astronomy Classification Scheme.* 47.63.-b, 47.11.-j.

Key words and phrases. Navier-Stokes equations, backflow stabilization, blood flow, finite element method.

Edited by
Weierstraß-Institut für Angewandte Analysis und Stochastik (WIAS)
Leibniz-Institut im Forschungsverbund Berlin e. V.
Mohrenstraße 39
10117 Berlin
Germany

Fax: +49 30 20372-303
E-Mail: preprint@wias-berlin.de
World Wide Web: http://www.wias-berlin.de/

Abstract

In computational simulations of fluid flows, instabilities at the Neumann boundaries may appear during backflow regime. It is widely accepted that this is due to the incoming energy at the boundary, coming from the convection term, which cannot be controlled when the velocity field is unknown. We propose a stabilized formulation based on a local regularization of the fluid velocity along the tangential directions on the Neumann boundaries. The stabilization term is proportional to the amount of backflow, and does not require any further assumption on the velocity profile. The perfomance of the method is assessed on a two- and three-dimensional Womersley flows, as well as considering a hemodynamic physiological regime in a patient-specific aortic geometry.

1 Introduction

Let us consider an incompressible fluid in a domain $\Omega \subset \mathbb{R}^d$, $d = 2,3$, whose boundary is decomposed as

$$\partial\Omega := \Gamma_{\text{in}} \cup \Gamma_{\text{out}} \cup \Sigma,$$

with Γ_{in} and Γ_{out} denoting the boundaries with Dirichlet data (i.e., known velocity profile) and Neumann data (i.e., known stresses), respectively. We consider an incompressible, Newtonian fluid, modeled through the incompressible Navier-Stokes equations for the velocity $\boldsymbol{u} : \Omega \times \mathbb{R}^+ \to \mathbb{R}^d$ and the pressure $p : \Omega \times \mathbb{R}^+ \to \mathbb{R}$:

$$\begin{cases} \rho\partial_t \boldsymbol{u} + \rho\boldsymbol{u}\cdot\boldsymbol{\nabla}\boldsymbol{u} - \boldsymbol{\nabla}\cdot\boldsymbol{\sigma}(\boldsymbol{u},p) = \boldsymbol{0} & \text{in} \quad \Omega, \\ \boldsymbol{\nabla}\cdot\boldsymbol{u} = 0 & \text{in} \quad \Omega, \\ \boldsymbol{u} = \boldsymbol{u}_{\text{in}} & \text{on} \quad \Gamma_{\text{in}}, \\ \boldsymbol{u} = \boldsymbol{0} & \text{on} \quad \Sigma, \\ \boldsymbol{\sigma}(\boldsymbol{u},p)\boldsymbol{n} = -p_{\text{out}}\boldsymbol{n} & \text{on} \quad \Gamma_{\text{out}}, \end{cases} \tag{1}$$

In (1), ρ stands for the fluid density, μ denotes the dynamic fluid viscosity and the fluid Cauchy-stress tensor is given by $\boldsymbol{\sigma}(\boldsymbol{u},p) := -p\boldsymbol{I} + 2\mu\boldsymbol{\varepsilon}(\boldsymbol{u})$ and $\boldsymbol{\varepsilon}(\boldsymbol{u}) := (\boldsymbol{\nabla}\boldsymbol{u} + \boldsymbol{\nabla}\boldsymbol{u}^{\text{T}})/2$. Furthermore, $\boldsymbol{u}_{\text{in}}$ represents a given velocity profile and p_{out} a given pressure data.

Let us denote with $(\cdot,\cdot)_X$ the usual scalar product in the Sobolev space $L^2(X)$, for $X \subset \mathbb{R}^d$, and with $\|\cdot\|_{0,X}$ the associated norm. Then, the quantities

$$E(t) := \frac{\rho}{2}\|\boldsymbol{u}\|^2_{0,\Omega}\ ,\ D(t) := 2\mu\|\boldsymbol{\varepsilon}(\boldsymbol{u}(s))\|^2_{0,\Omega}$$

denote the total (purely kinetic) energy of the 3D fluid system given by (1) and the dissipative effects, respectively. Using standard arguments, in the case of an isolated system, i.e., $\boldsymbol{u}_{\text{in}} = \mathbf{0}$ and $p_{\text{out}} = 0$, the energy balance of system (1) yields

$$d_t E(t) = -D(t) - \left(\frac{\rho}{2}|\boldsymbol{u}|^2, \boldsymbol{u}\cdot\boldsymbol{n}\right)_{\Gamma_{\text{out}}}. \tag{2}$$

Notice that the last term of the right hand side of (2) cannot be bounded, when the velocity profile at the outlet is unknown. Hence, a stable energy balance cannot be guaranteed a priori during backflow, i.e., when $\boldsymbol{u}\cdot\boldsymbol{n} < 0$ on Γ_{out}. This issue typically arises when cutting the physical domain and imposing Neumann boundary conditions (as in Problem (1)), which do not consider the physical convective effects present in the neglected parts of the physical domain. In practice, this might cause large unphysical oscillations in the velocity near the outlet, compromising the stability, the feasability and the reliability of the numerical simulations (see, e.g., Figure 1).

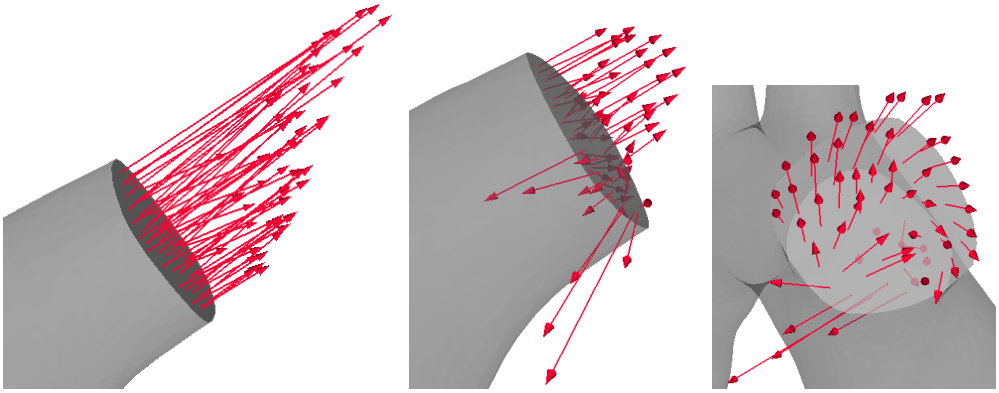

Figure 1: A typical backflow instability arising in blood flow simulations: velocity vectors on the outlets at the time of peak outflow (left) and the time when backflow starts in the first outlet (center and right).

Different treatments to overcome this problem have been already proposed in the literature. A first group of methods consist in imposing additional constraints on the velocity field at the Neumann boundary, e.g. via enforcing the shape of the velocity profile. Due to the global mass conservation, this directly controls the magnitude of the velocity field on Γ_{out}, ensuring the overall stability. However, this shape constraint has to be imposed through Lagrange multipliers [16], which might involve considerable modifications of the numerical solver and might increase the overall computational cost. Simpler variants consist in constraining only the direction of the flow on the Neumann boundaries, for example enforcing the outlet velocity to be normal to the boundary. This approach can reduce the oscillations, but it does not necessarely eliminate them [7].

A second group of methods is based on achieving stability imposing the total outlet pressure $\boldsymbol{\sigma}(\boldsymbol{u}, p)\boldsymbol{n} = p_{\text{out}} + \rho|\boldsymbol{u}|^2/2$ at the open boundary, hence modifying the Neumann boundary condition $(1)_5$ (see, e.g., [9]). However, this might lead to unphysical

solutions [13]. Inspired from [15, 14], a similar strategy consists in modifiying the Neumann boundary condition $(1)_5$ as

$$\boldsymbol{\sigma}(\boldsymbol{u},p)\boldsymbol{n} = -\bar{p}_{\text{out}}\boldsymbol{n} + \beta\,\frac{\rho}{2}\,|\boldsymbol{u}\cdot\boldsymbol{n}|_{-}\,\boldsymbol{u} \quad \text{on} \quad \Gamma_{\text{out}}\,, \tag{3}$$

with

$$|\boldsymbol{u}|_{-} := \frac{\boldsymbol{u}-|\boldsymbol{u}|}{2}\,,\ \beta \geq 0, \tag{4}$$

so that the Neumann condition is only perturbed in the presence of backflow. In particular, two variants of this method were recently reported. The first, developed in [7, 3] in the context of hemodynamics, is based on the choices $\beta \leq 1.0$ and $\bar{p}_{\text{out}} = p_{\text{out}}$, and will be denoted in what follows as *inertial stabilization*. The second, using $\beta = 1$ and $\bar{p}_{\text{out}} = p_{\text{out}} + f(U,Q)\rho/2$, has been proposed in [10] for respiratory mechanics and it is also suitable for blood flows. Here, $f(U(\mathbf{x}),Q)$ corresponds to an approximation of $|\boldsymbol{u}\cdot\boldsymbol{n}|_{-}\,\boldsymbol{u}$, based on a assumed velocity profile $U(\mathbf{x})$ on the open boundary and a given - or computed - flux Q, allowing the simultaneous imposition of pressure and flows rates. Note that, for all these techniques, the global stability is ensured if $\beta = 1$, according to Equation (2).

The aim of this work is to propose a new stabilized formulation, based on a local regularization of the fluid velocity along the tangential directions on the Neumann boundaries. The stabilization consists in a symmetric penalization of the tangential variation of the outlet velocity, proportional to the amount of backflow, and it does not require any assumption on the velocity profile.

The rest of the paper is organized as follows. The tangential regularization is introduced in Section 2. In Section 3 the performance of the method is assessed through extensive numerical examples in the blood flow regime. In order to explain the behaviour observed in the numerical examples, Section 4 discusses a possible analytical estimation of the stabilization parameter in terms of the mesh size. Finally, Section 5 draws the conclusions.

2 Tangential regularization for backflow stabilization

2.1 Formulation

Let us consider the standard Sobolev spaces on Ω, $L^2(\Omega)$ and $H^1(\Omega)$, and let us define

$$H^1_0(\Omega) := \left\{\boldsymbol{v} \in H^1(\Omega) \mid \boldsymbol{v} = \boldsymbol{0} \text{ on } \Gamma_{\text{in}} \cup \Sigma\right\}. \tag{5}$$

The variational form of Problem (1) reads: Find $\boldsymbol{u} \in H^1(\Omega)$ satisfying $(1)_{3-4}$, and $p \in L^2(\Omega)$ such that

$$\begin{cases} \mathcal{A}(\boldsymbol{v},\boldsymbol{v}) - \mathcal{B}(p,\boldsymbol{v}) = -\left(p_{\text{out}}\boldsymbol{n},\boldsymbol{v}\right)_{\Gamma_{\text{out}}}, \\ \qquad\qquad \mathcal{B}(q,\boldsymbol{u}) = 0, \end{cases} \tag{6}$$

for all $\boldsymbol{v} \in H^1_0(\Omega)$ and $q \in L^2(\Omega)$, with

$$\mathcal{A}(\boldsymbol{u},\boldsymbol{v}) := \rho\,(\partial_t \boldsymbol{u},\boldsymbol{v})_\Omega + \rho\,(\boldsymbol{u}\cdot\boldsymbol{\nabla}\boldsymbol{u},\boldsymbol{v})_\Omega + 2\mu\,(\boldsymbol{\varepsilon}(\boldsymbol{u}),\boldsymbol{\varepsilon}(\boldsymbol{v}))_\Omega\,, \quad \mathcal{B}(p,\boldsymbol{v}) := (p,\boldsymbol{\nabla}\cdot\boldsymbol{v})_\Omega\,. \tag{7}$$

Note that, setting $\boldsymbol{v} = \boldsymbol{u}$, we obtain the energy balance (2) for the nonforced system. Motivated by the fact that (2) does not allow a control *a priori* on the energy, in order to avoid the arise of artificial oscillations we propose to modify the weak formulation $(6)_1$ as

$$\mathcal{A}(\boldsymbol{u},\boldsymbol{v}) + \frac{\rho}{2}\sum_{j=1}^{d-1}\mathcal{T}_j(\boldsymbol{u},\boldsymbol{v}) - \mathcal{B}(p,\boldsymbol{v}) = -\left(p_{\text{out}}\boldsymbol{n},\boldsymbol{v}\right)_{\Gamma_{\text{out}}}, \tag{8}$$

with the dissipative terms

$$\mathcal{T}_j(\boldsymbol{u},\boldsymbol{v}) := \left(\gamma|\boldsymbol{u}\cdot\boldsymbol{n}|_-\,\boldsymbol{t}_j^\intercal\boldsymbol{\nabla}\boldsymbol{u},\boldsymbol{t}_j^\intercal\boldsymbol{\nabla}\boldsymbol{v}\right)_{\Gamma_{\text{out}}}. \tag{9}$$

In (9), the vectors $\boldsymbol{t}_j$, $j = 1,\dots,d-1$ stand for the tangential directions to Γ_{out}, $\gamma \in \mathbb{R}^+$ is a stabilization parameter and $|\boldsymbol{u}\cdot\boldsymbol{n}|_-$ is the negative part of the normal velocity, defined as in (4).

We observe that the modified variational formulation (8) formally restricts the space of the velocity solution to

$$H^1_{\mathcal{T}} := \left\{\boldsymbol{v} \in H^1(\Omega) \mid (\nabla\boldsymbol{v})|_{\Gamma_{\text{out}}} \in L^2(\Gamma_{\text{out}})\right\} \subset H^1(\Omega)$$

However, it is worth noticing that this condition is much less restrictive than, e.g., enforcing directly the shape or the direction of the velocity profile on the Neumann boundary Γ_{out}.

Remark 1 *The choice of penalizing the tangential derivatives is motivated by the observation that velocity instability typically arises along the open boundary. It is worth noticing that this term is not consistent with the Navier-Stokes equations, for example it does not reproduce a Womersley flow exactly. Other options, like the penalization of the normal derivative instead of the tangential ones -a strategy which would be consistent with the Womersley solution - have been also tested, without achieving a stable solution. The choice of the tangential derivative will be better clarified also in the stability analysis presented in the next sections.*

2.2 Energy balance

The energy balance for the modified variational formulation (8) reads

$$d_t E(t) = -D(t) - \frac{\rho}{2}\int_{\Gamma_{\text{out}}}\left\{(\boldsymbol{u}\cdot\boldsymbol{n})|\boldsymbol{u}|^2 - |(\boldsymbol{u}\cdot\boldsymbol{n})|_-\gamma\sum_{j=1}^{d-1}|\boldsymbol{t}_j^\intercal\boldsymbol{\nabla}\boldsymbol{u}|^2\right\}d\Gamma\,. \tag{10}$$

Let us decompose the outlet boundary as $\Gamma_{\text{out}} = \Gamma_b \cup \Gamma_o$, where $\Gamma_b := \{x \in \Gamma_{\text{out}} \mid \boldsymbol{u}(x) \cdot \boldsymbol{n} < 0\}$ (backflow boundary), and $\Gamma_o := \Gamma_{\text{out}} \backslash \Gamma_b$ (outflow boundary). We can rewrite the energy estimate (10) as

$$d_t E(t) = -D(t) - \frac{\rho}{2} \int_{\Gamma_o} (\boldsymbol{u} \cdot \boldsymbol{n}) |\boldsymbol{u}|^2 \, d\Gamma - \frac{\rho}{2} \underbrace{\int_{\Gamma_b} |\boldsymbol{u} \cdot \boldsymbol{n}| \left(\gamma |\boldsymbol{t} \boldsymbol{\nabla} \boldsymbol{u}|^2 - |\boldsymbol{u}|^2 \right) d\Gamma}_{\mathcal{E}}. \tag{11}$$

The term $\mathcal{E}$, denoting the energy injection due to backflow, can be estimated as

$$\mathcal{E} \geq C(\boldsymbol{u}) \int_{\Gamma_b} \left(\gamma |\boldsymbol{t} \boldsymbol{\nabla} \boldsymbol{u}(x)|^2 - |\boldsymbol{u}(x)|^2 \right) d\Gamma \, , \tag{12}$$

where $C(\boldsymbol{u}) > 0$ is a constant which depends on $\boldsymbol{u}$. Thus, the regularization terms (9) allow to achieve a stability in the sense of energy ($\mathcal{E} > 0$) under the condition

$$\int_{\Gamma_b} |\boldsymbol{u}|^2 d\Gamma < \int_{\Gamma_b} \gamma \sum_{j=1}^{d-1} |\boldsymbol{t}_j^{\intercal} \boldsymbol{\nabla} \boldsymbol{u}|^2 d\Gamma. \tag{13}$$

Note that the existence of a parameter $\gamma \geq 0$, such that the condition (13) is satisfied, is ensured by the Poincaré's lemma, since, by construction, $\boldsymbol{u} = \boldsymbol{0}$ on $\partial\Gamma_b$. Moreover, defining (9) based on the penalization of the normal derivative as discussed in Remark 1, would not allow to apply Poincaré's lemma straightforwardly .

2.3 Time semi-discretization

The time discretization of the stabilization term $\mathcal{T}_j$ has to be consistent with the one used for the convective term $\boldsymbol{u} \cdot \boldsymbol{\nabla} \boldsymbol{u}$. Denoting the time discretized convection with $\boldsymbol{u}^* \cdot \boldsymbol{\nabla} \boldsymbol{u}^n$, n being the current time step, the tangential regularization terms should be defined as

$$\mathcal{T}_j(\boldsymbol{u}^n, \boldsymbol{v}) := \left(\gamma |\boldsymbol{u}^* \cdot \boldsymbol{n}|_- \boldsymbol{t}_j^{\intercal} \boldsymbol{\nabla} \boldsymbol{u}^n, \boldsymbol{t}_j^{\intercal} \boldsymbol{\nabla} \boldsymbol{v} \right)_{\Gamma_{\text{out}}},$$

in order to maintain an energy balance analogous to (10), also in the time semi-discrete framework. In particular, using a semi-implicit approach for the convection, i.e. $\boldsymbol{u}^* = \boldsymbol{u}^{n-1}$, the regularization does not introduce any further nonlinearity in the problem.

3 Numerical experiments for blood flows

3.1 2D Womersley flow

The first set of benchmarks is based on a two-dimensional Womersley flow, describing the solution to the time-dependent Navier-Stokes equations in the rectangular domain

$\Omega := [0, 2R] \times [0, L] \subset \mathbb{R}^2$, driven by an oscillating pressure gradient

$$\frac{\partial p}{\partial x} = 0 \, , \; \frac{\partial p}{\partial y} = -\frac{\delta p}{L} \sin(\omega t) \, ,$$

for a given pressure drop δp and a given frequency ω. In particular, since the velocity profile does not vary along the y direction, there is no physical convection and thus the Navier-Stokes solution matches the solution of the corresponding Stokes problem.

For all numerical examples in this section, we set the physical constants to $\rho = 1$ g/cm^3, $\mu = 0.035$ Po, $L = 5$ cm, $R = 1$ cm, $\delta p = 2666$ dyn/cm^2, $\omega = 4\pi$ rad/s, corresponding to typical values for arterial blood flows. We impose the analytical velocity profile as a Dirichlet boundary condition on $y = 0$, and $p_{\text{out}} = 0$ on $y = L$. The Navier-Stokes equations are solved numerically through a finite element method with monolithic-$(\boldsymbol{u}, p)$ time marching-scheme, implemented in FreeFem++ [12]. In particular, we employ stabilized $\mathbb{P}_1/\mathbb{P}_1$ velocity/pressure finite element spaces. The time step is chosen as $\tau = 0.002$ s, and the convective term is semi-discretized as in Section 2.3.

The velocity profiles resulting from the stabilized formulation, compared with the Stokes solution – which agrees with the analytical solution presented in [8] – are shown in Figure 2 for two different mesh sizes. We also compare our approach against the inertial stabilization (3), showing in both cases the velocity profile obtained with the smallest stabilization parameters (γ for the proposed tangential regularization, β for the inertial stabilization), so that the simulation remained stable. The tangentially regularized solution seems to better approximate the Stokes profile in all cases. Moreover, in Figure 2 (bottom), we also illustrate how the different stabilizations perturb the pressure profiles at both inlet and outlets, and we do not observe any relevant differences between both approaches.

It is worth noticing that refining the computational mesh allows to reduce the size of the stabilization parameters. This could be explained by the fact that, since in a Womersley flow the convection is a purely numerical artifact, in the continuous limit no stabilization is needed. We will observe later the same behavior also in more complex examples, and we will sketch in Section 4 how the energy of spurious oscillations can be controlled through a stabilization parameter depending on the mesh element size.

Remark 2 *Further numerical results suggested that the tangential stabilization parameter can also be reduced when increasing the approximation order of the velocity, for example when using $\mathbb{P}_2$ elements. A similar feature was not observed for the inertial stabilization, see Figure 3.*

3.2 3D Womersley flow

As a next step towards realistic physiological regimes, we consider a 3D Womersley flow in a cylindrical domain of radius $R = 1$ cm and length $L = 5$ cm, subject to an

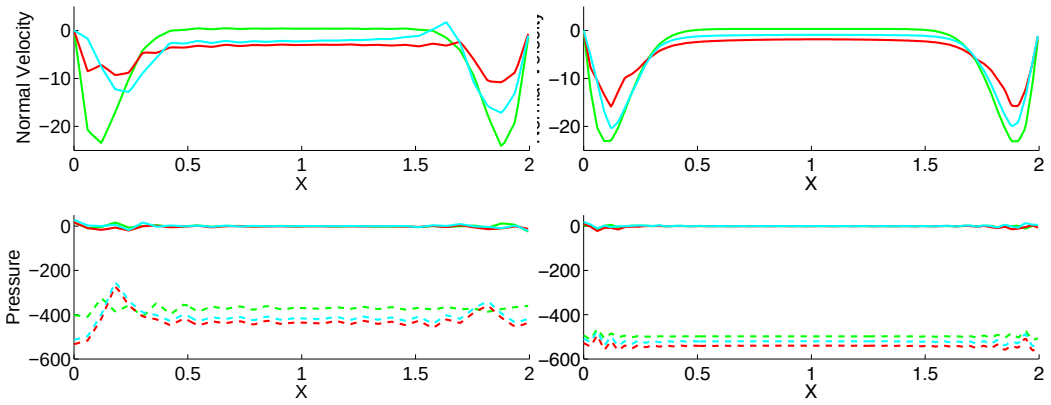

(a) $h = 0.06$: $\beta = 0.3$ v/s $\gamma = 0.0008$ (b) $h = 0.03$: $\beta = 0.1$ v/s $\gamma = 0.0001$

Figure 2: Velocity (top) and pressure profiles (bottom) at $t = 0.5s$ on the Neumann boundary with $\mathbb{P}_1/\mathbb{P}_1$ elements for the 2D-Womersley example, comparing the Stokes solution (green), inertial stabilization (red) and tangential regularization (cyan). The dashed pressure curves represent the profiles in the Dirichlet boundary, while continuous lines correspond to the results on the Neumann boundary.

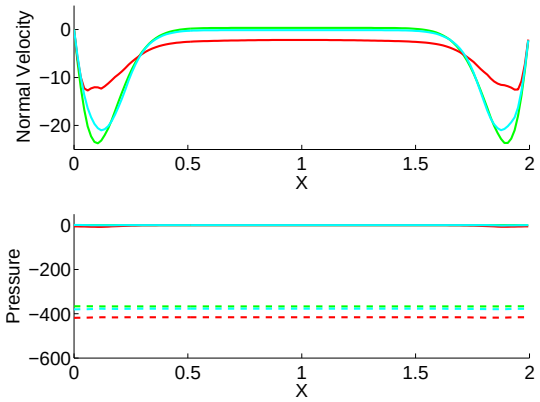

Figure 3: Velocity (top) and pressure (bottom) profiles at $t = 0.5s$ on the Neumann boundary using $\mathbb{P}_2/\mathbb{P}_1$ elements for the 2D-Womersley example, comparing the Stokes solution (green), inertial stabilization (red) and tangential regularization (cyan), for $h = 0.06$, $\beta = 0.1$ and $\gamma = 0.00003$.

oscillating pressure drop of amplitude $\delta p = 2000$ dyn/cm^2. The other parameters are chosen as in the two dimensional case. For the numerical solution, we emploied a non-incremental Chorin-Temam projection method [6, 11, 18] for solving the Navier-Stokes equations. The discretization was based on a time-step of 0.002 s, $\mathbb{P}_1/\mathbb{P}_1$ finite element spaces for velocity and pressure and an SUPG stabilization for the

convection [5].

The simulations were setup as follows: first, a Stokes simulation (validated against the periodic analytical solution, see, e.g., [8]) was run with a given pressure gradient $(\delta p/L)\sin\omega t$ between inlet and outlet. The resulting velocity profile was used as Dirichlet boundary condition at the inlet for the Navier-Stokes simulations, while a homogeneous pressure was enforced at the outlet.

The results, summarized in Figure 4, show a similar behavior as in the 2D case. Refining the mesh improves the approximation and the tangential regularization performs better than the inertial stabilization, in terms of the outlet velocity profile.

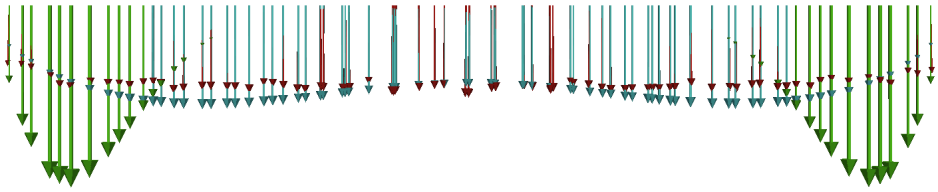

(a) $h = 0.06$: Stokes (green), NS with $\gamma = 0.001$ (cyan), NS with $\beta = 0.1$ (red)

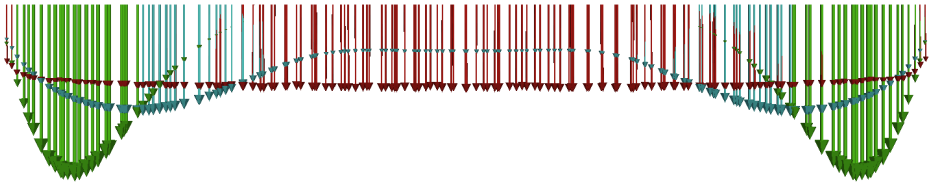

(b) $h = 0.03$: Stokes (green), NS with $\gamma = 0.0002$ (cyan), NS with $\beta = 0.05$ (red)

Figure 4: Velocity profiles at $t = 1s$ (peak backflow) on the Neumann boundary for the 3D-Womersley example, comparing the Stokes solution (green), stabilization with (3) (red) and tangential regularization (cyan).

3.3 3D Patient specific aorta

Our next example consists in the simulation of the blood flow in a patient-specific aorta, obtained from the euHeart database (`www.euheart.eu`), see Figure 5. The geometry was segmented from medical images using a segment growing registration algorithm [1, 2], and the finite element mesh was generated using 3-matic (Materialise, Leuven, Belgium) and TetGen [17]. For the numerical simulations, we considered two different level of refinement for the computational mesh (Figure 5), denoted in what follows as *coarse* (52K tetrahedra, 10K nodes, maximum element size $h_{\max}$= 0.11 cm) and *fine* (320K tetrahedra, 60K nodes, maximum element size $h_{\max}$= 0.055 cm).

At the inlet boundary (ascending aorta), we impose a plug flow profile with amplitude based on the PC-MRI measured flow rate from the same patient (peak flow rate of 350 cm^3/s). At the outlets, three-elements Windkessel models where used to

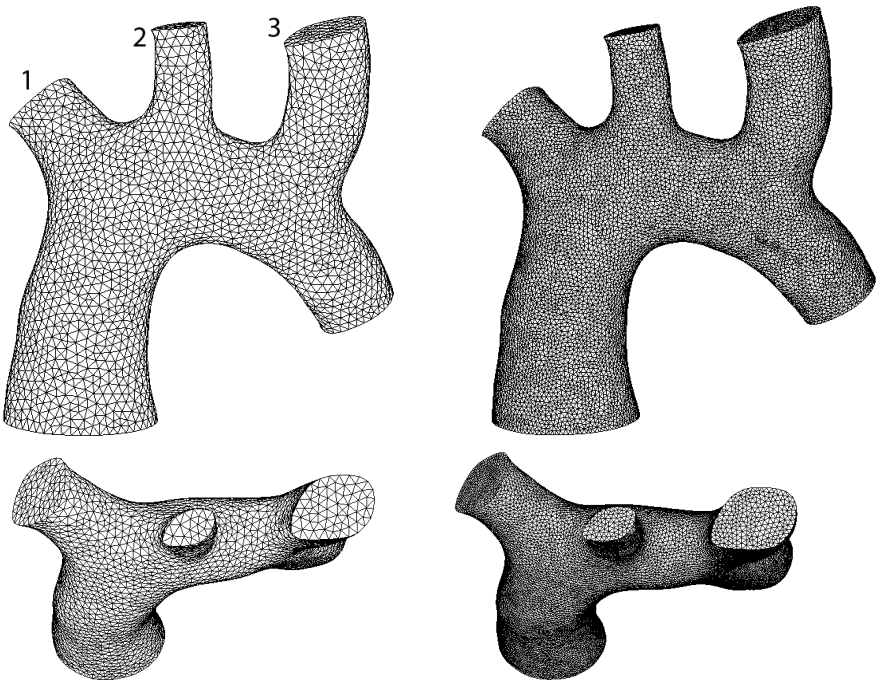

Figure 5: Frontal and top views of the coarse (left) and fine (right) meshes for the patient-specific aorta geometry. The outlets (1 to 3) are numbered according to the initial direction of the flow.

represent the effect of the neglected downstream circulation, calibrated in order to approximate the available measured pressures and the measured flows on each outlet [4].

Figures 6, 7 and 8 show the snapshots of the velocity at the selected instants during backflow for three different Neumann boundaries. In each case, we compare the results without regularization and with the minimal value of the stabilization parameter γ, for which the spurious oscillations have been removed. We observe that also in this example, where the physical convection is important, we are able to choose a smaller stabilization parameter when the characteristic mesh element size decreases.

4 On the stabilization of spurious oscillations in finite element solutions

In this section, we will investigate how the control of spurious oscillations through the regularization parameter γ, can be related to the element size h.

Let us first restrict to the two-dimensional case. We assume that on the open boundary we have a “spurious” velocity field, i.e., uncorrelated values of the velocity with support contained in two (in general in a few) boundary elements, e.g. as depicted in Figure 9.

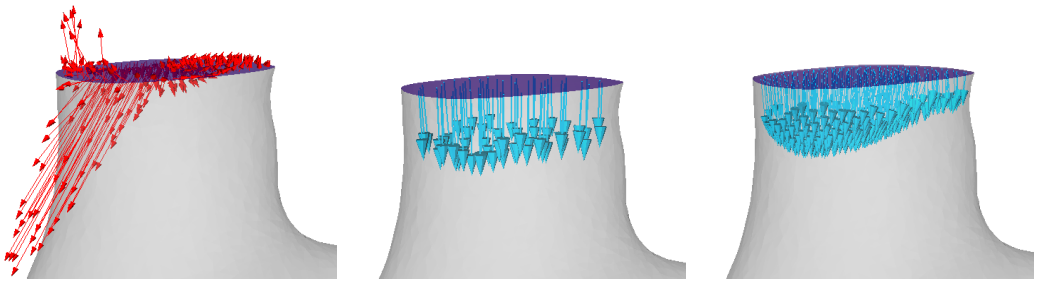

Figure 6: Patient-specific aorta: velocity vectors on the first outlet at time $t = 0.34$s. Left: fine mesh, without regularization. Center: coarse mesh, regularization with the minimum values of $\gamma = 0.0025$. Right: fine mesh, regularization with the minimum values of $\gamma = 0.0008$.

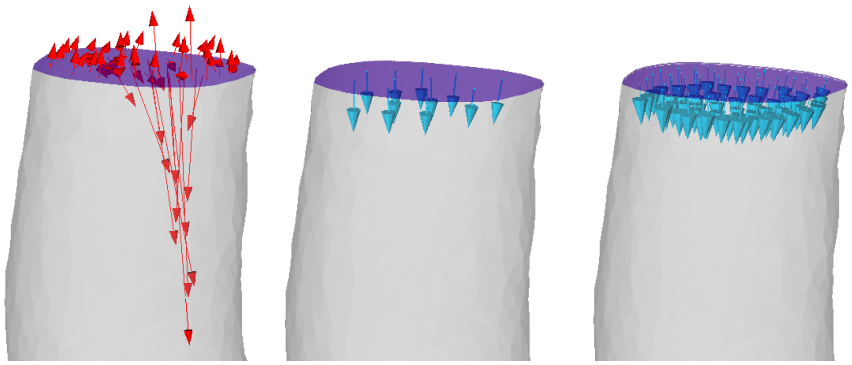

Figure 7: Patient-specific aorta: velocity vectors on the second outlet at time $t = 0.39$s. Left: fine mesh, without regularization. Center: coarse mesh, regularization with the minimum values of $\gamma = 0.0025$. Right: fine mesh, regularization with the minimum values of $\gamma = 0.0008$.

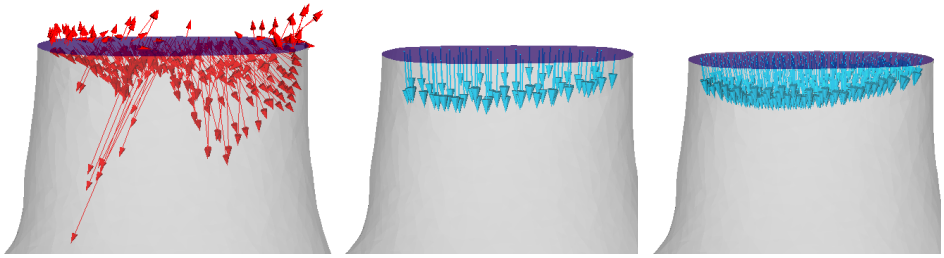

Figure 8: Patient-specific aorta: velocity vectors on the third outlet at time $t = 0.39$s. Left: fine mesh, without regularization. Center: coarse mesh, regularization with the minimum values of $\gamma = 0.0025$. Right: fine mesh, regularization with the minimum values of $\gamma = 0.0008$.

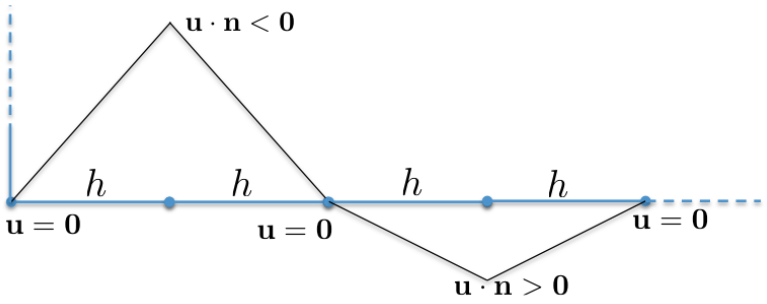

Figure 9: A sketch of spurious oscillations arising at an open boundary, in the case of piecewise linear finite elements for the velocity.

For the configuration depicted in Figure 9, we can directly compute the value of γ which satisfies piecewise the stability condition (13) for each subdomain of Γ_b where the support of $\boldsymbol{u}$ is an interval of length $2h$, namely

$$\int_0^{2h} |\boldsymbol{u}|^2 dx < \int_0^{2h} \gamma |\partial_x \boldsymbol{u}|^2 dx, \tag{14}$$

by replacing $u = u_n x/h$ for $0 \le x \le h$ and $u = u_n(2h-x)/h$ for $0 \le x \le h$. This yields

$$\int_0^h x^2/h^2 dx + \int_h^{2h} (2h-x)^2/h^2 dx < \gamma/h^2 \tag{15}$$

$$\int_0^h x^2 dx + \int_h^{2h} (2h-x)^2 dx < \gamma 2h \tag{16}$$

$$h^2/3 < \gamma. \tag{17}$$

Note that, by construction, in this configuration the stabilization parameter γ term does not depend on the amplitude of the velocity field. In three dimensions, a similar dependency of the parameter γ on h can be obtained analogously by assuming a support of the spurious velocity of $\mathcal{O}(h)$, so that the condition (13) can be directly related to Poincaré's inequality, yielding $\gamma = \mathcal{O}(h^2)$.

5 Conclusions

We presented a backflow stabilization technique for incompressible fluid simulations, based on a tangential regularization of the velocity field, which fits naturally within a standard finite element formulation. The proposed formulation has been assessed through several numerical tests, considering two- and three-dimensional Womersley problems, and blood flow through a patient-specific aorta.

As an additional outcome of the numerical tests, we observed that the size of the stabilization parameter may decrease with the mesh size. The analysis of a simplified configuration showed that a stabilization parameter $\gamma = \mathcal{O}(h^2)$ can be chosen in order to control the energy induced by purely spurious oscillations in the velocity profile. This behavior is in fact in agreement with the numerical experiments.

Future work will consist in the extension to respiratory mechanics. In the airflow regime, since the dynamic pressure is much larger than the static one, a careful treatment of the boundary condition is necessary, in order to achieve a satisfactory accuracy of the overall pressure field. A possible generalization of the tangential regularization could be based on including a correction term for the outlet velocity profile, similarly to what has been proposed in [10] in the case of inertial stabilization.

6 Acknowledgements

We sincerely acknowledge Jean-Frédéric Gerbeau, Miguel A. Fernández (INRIA Paris Rocquencourt), and Mahmoud Ismail and Volker Gravemeier (TU München) for valuable discussions during the preparation of the manuscript. We are grateful to Philipp Beerbaum and Israel Valverde (King's College London) for the acquisition of the patient data, and David Barber, Rod Hose and Cristina Staicu (University of Sheffield) for the segmented aortic geometry. This research was performed in the European CommunityÕs Seventh Framework Programme (FP7/2007-2013) under grant agreement no.224495 (euHeart project).

References

[1] D.C. Barber, E. Oubel, A.F. Frangi, and D.R. Hose. Efficient computational fluid dynamics mesh generation by image registration. *Med. Image Anal.*, 11(6):648–662, 2007.

[2] D.C. Barber, C. Staicu, I. Valverde, P. Beerbaum, and D.R. Hose. Registration based segment growing for vascular segmentation. *IEEE T Med Imaging*, 2012. Submitted.

[3] Y. Bazilevs, J.R. Gohean, T.J.R. Hughes, R.D. Moser, and Y. Zhang. Patient-specific isogeometric fluid-structure interaction analysis of thoracic aortic blood flow due to implantation of the Jarvik 2000 left ventricular assist device. *Comput. Methods Appl. Mech. Engrg.*, 198(45-46):3534–3550, 2009.

[4] Cristóbal Bertoglio. *Forward and Inverse Problems in Fluid-structure Interaction. Application to Hemodynamics*. Ph.D. Thesis, Université Pierre et Marie Curie - Paris VI, November 2012.

[5] A.N. Brooks and T.J.R. Hughes. Streamline upwind/Petrov-Galerkin formulations for convection dominated flows with particular emphasis on the incompressible Navier-Stokes equations. *Comp. Meth. App. Mech. Eng.*, 32:199–259, 1982.

[6] A.J. Chorin. On the convergence of discrete approximations to the Navier-Stokes equations. *Math. Comp.*, 23:341–353, 1969.

[7] M. Esmaily Moghadam, Y. Bazilevs, T.-Y. Hsia, I. Vignon-Clementel, A. Marsden, and Modeling of Congenital Hearts Alliance. A comparison of outlet boundary treatments for prevention of backflow divergence with relevance to blood flow simulations. *Computational Mechanics*, 48:277–291, 2011. 10.1007/s00466-011-0599-0.

[8] L. Formaggia, J-F. Gerbeau, F. Nobile, and A. Quarteroni. Numerical treatment of defective boundary conditions for the Navier-Stokes equations. *SIAM J. Numerical Analysis*, 40(1):376–401, 2002.

[9] L. Formaggia, A. Moura, and F. Nobile. On the stability of the coupling of 3D and 1D fluid-structure interaction models for blood flow simulations. *M2AN Math. Model. Numer. Anal.*, 41(4):743–769, 2007.

[10] V. Gravemeier, A. Comerford, L. Yoshihara, M. Ismail, and W.A. Wall. A novel formulation for Neumann inflow boundary conditions in biomechanics. *International Journal for Numerical Methods in Biomedical Engineering*, 28(5):560–573, 2012.

[11] J.-L. Guermond, P. Minev, and J. Shen. An overview of projection methods for incompressible flows. *Comput. Methods Appl. Mech. Engrg.*, 195:6011–6045, 2006.

[12] F. Hecht, O. Pironneau, A. Le Hyaric, and K. Ohtsuka. *FreeFem++ v. 2.11. User's Manual*. University of Paris 6, 2010.

[13] J.G. Heywood, R. Rannacher, and S. Turek. Artificial boundaries and flux and pressure conditions for the incompressible Navier–Stokes equations. *International Journal for Numerical Methods in Fluids*, 22:325–352, 1996.

[14] Thomas JR Hughes and Garth N Wells. Conservation properties for the galerkin and stabilised forms of the advection–diffusion and incompressible navier–stokes equations. *Computer methods in applied mechanics and engineering*, 194(9):1141–1159, 2005.

[15] T.J.R. Hughes, L.P. Franca, and G.M. Hulbert. A new finite element formulation for computational fluid dynamics: Viii. the galerkin/least-squares method for advective-diffusive equations. *Comp. Methods Appl. Mech. Engrg.*, 73(2):173–189, 1989.

[16] HJ Kim, CA Figueroa, TJR Hughes, KE Jansen, and CA Taylor. Augmented lagrangian method for constraining the shape of velocity profiles at outlet boundaries for three-dimensional finite element simulations of blood flow. *Comp. Methods Appl. Mech. Engrg.*, 198(45):3551–3566, 2009.

[17] H. Si. Adaptive tetrahedral mesh generation by constrained Delaunay refinement. *Int. J. Numer. Meth. Engrg.*, 75:856–880, 2008.

[18] R. Temam. Une méthode d'approximation de la solution des équations de Navier-Stokes. *Bull. Soc. Math. France*, 96:115–152, 1968.